



Modelling the Effect of Lateral Inertia on the Dynamic Response of Aluminium Square Tube Extrusions

O. T. Shitta-Bey^{1,*}, A. E. Olorunnisola², and O. Olatunbosun³,

^{1,2,3}Vehicle Safety Research Group, Department of Mechanical Engineering, University of Lagos, Lagos State, NIGERIA

Abstract

Crashworthiness of automobiles require the design of crush tubes installed as a frontal structure to absorb energy by deforming plastically during collision. The crushing behaviour of aluminium extrusions modelled as square tubes is investigated under quasi-static and dynamic loading conditions using the non-linear explicit finite element code LS DYNA. Previous works have attributed the dynamic increase of the peak and mean crushing load of aluminium thin-walled structures under axial compression, to inertia effects. Results of our investigation revealed that there is a considerable thickening of the shell side walls before and during progressive folding. This shell thickening is established as the cause of lateral inertia which consequently results in increased crush strength. In addition, a positive correlation was established between the shell thickening and crushing speeds.

Keywords: Aluminum, Square-Tube, Dynamic, Lateral Inertia, Thickening, Thin-walls

1.0 INTRODUCTION

Aluminum square tube extrusions used as energy-absorbing members have received vast research attention over the years, due to the weight savings and cost optimization that can be achieved when they are used in different engineering products. The applications of aluminium extrusions have been expanding since the 1960s. Unlike steel, aluminium can be extruded in complicated cross-sectional shapes with varying wall thickness distribution [1]. Different energy absorbing devices are provided in different practical applications to mitigate the effect of adverse reaction force on other members of the assembly. Some of the popular areas of application include automotive [2], train [3], aircraft [4], nuclear engineering [5], and marine crashworthiness [6].

The dynamic behavior of tubes used as energy absorbers, has been studied extensively with attention on different performance parameters. Classical works were aimed at developing theoretical models for predicting the crush behavior of the tubes. Alexander [7] derived an approximate model for predicting the collapse load of a cylindrical tube. The investigation was aimed at developing a relationship expressing the allowable load

during energy absorption of cylindrical shells in vertical fuel channels of nuclear reactors.

Abramowicz [8], went further to derive a simplified theoretical model for determining the effective crushing distance of compressed thin walled columns with hardening property included in the material definition unlike previous works where perfectly plastic materials were considered. The energy dissipation during the crushing of energy-absorbing tubes was explained by Wierzbicki [9]. It was revealed that one-third of the energy is dissipated in the formation of extensional deformation mode and the remaining two-thirds is dissipated in equal proportions from the in extensional deformations of stationary and moving hinge lines.

Abramowicz and Jones [10], developed a theoretical relationship to predict the mean crushing load P_m of square tubes as expressed in equation 1.

$$P_m = K \sigma_o(t)^{5/3}(b)^{1/3} \quad (1)$$

where $K = 13.06$ for square tubes, σ_o is the flow stress, t is the tube thickness and b is the tube width.

Crashworthiness research, over the years, has been performed by experimental, analytical and numerical methods. Finite element simulation enables researchers develop and optimize different configurations and material models in understanding the performance behaviour of test specimen. Langseth and Hopperstad [11] performed a numerical investigation on the behaviour of the aluminium

*Corresponding author (Tel: +234 (0) 7069632068)

Email addresses: mea98ots@yahoo.com (O. T. Shitta-Bey), oluomosola@gmail.com (A. E. Olorunnisola), and remiolat@gmail.com (O. Olatunbosun)

alloy AA6060 with the finite element code LS DYNA. The model was validated with experimental findings from their previous work [12]. Under quasi-static and lower impact velocities, progressive folding was observed whilst under higher impact velocities, global buckling was observed. The test was performed within the range 8.47m/s to 19.85m/s under an impact mass of 55.92kg. It was suggested that lateral inertia effects were responsible for the different failure modes observed at the same impact energy but varying velocities.

Karagiozov and Jones [13] investigated the effects of axial and lateral inertia on the crushing behaviour of square aluminium tubes with velocity values within the range 14.84m/s to 98.27m/s. Lateral inertia was observed to significantly influence the crushing distance and energy absorption performance of the square tube via the elastic and plastic stress wave propagation along the tube wall. Again, it is suggested that lateral inertia has a significant effect on the development of the buckling shape and energy absorption performance of a tube. The crushing distance was shown to decrease as impact velocity increased at a constant impact energy of 600J.

Different authors have measured the crash performance of thin-walled tubes of different material and geometry with parameters such as the total energy absorption, specific energy absorption, crush force efficiency, peak and mean force, with dynamic effects attributed to inertia and/or strain rate sensitivity. This study attempts to investigate this underlying cause of lateral inertia along the walls of square aluminum extrusions under dynamic impact. The crushing behavior of aluminum extrusions modelled as square tubes was numerically tested under quasi-static and dynamic loading conditions using a non-linear explicit finite element code (LS DYNA). The lateral inertia effect is further investigated for an impact velocity range of 5m/s to 25m/s and an impact mass range of 10kg to 100kg

2.0 MATERIALS AND METHODS

2.1 Model Formulation

The models used for this investigation were based on the experimental data presented by Langseth et al [12] for the quasi-static and dynamic crushing of aluminum square tube extrusions. The tubes were modelled as 80 x 80mm aluminum A6060 alloys of temper T4 and T6 with thickness from 1.8 to 2.5 mm.

The full model although computationally expensive, was built using the Belytschko-Lin-Tsay shell element of 5 x 5mm element size. The Belytschko-Lin-Tsay shell element was used with five integration points through the thickness of the tube and one point in the plane of the elements due to nonlinearity of the material

property. The “Auto Mesher” keyword was used to discretize the model with a mesh size of 5 mm resulting in a total of 3968 elements and 4212 nodes. The striker or impacting mass was modelled as a rigid member.

2.2 Imperfection

The trigger was characterized by a half sine wave from the beginning to end of a side wall. The mathematical expression of the trigger is given by equation 2,

$$\beta(x) = \beta_0 [\sin(\pi y/b)] \tag{2}$$

where β_0 is the amplitude of the trigger, b is the width of the tube, x and y are the nodal coordinates. The nodal displacement values along the shell wall were generated from the equation with the amplitude, tube width and step size along the y direction as primary input parameters. Figure 1 shows the trigger position for the 2.5 mm tube of temper T4.

2.3 Material Model

LS DYNA is equipped with a robust library of material models that reflect the properties and behaviour of different materials. Commonly used in the simulation of the response of energy-absorbing materials include the plastic kinematic model, MAT_3 [14], the piecewise linear plasticity model, MAT_024 [15], and the anisotropic plasticity model, MAT_103 [16]. In the present work, the aluminium alloy was modelled as an elasto-plastic material. MAT_024 (piecewise linear plasticity) material model was used to model the AA6060 alloy of temper T4 and T6. The MAT_024 keyword allows an arbitrary stress strain curve and an arbitrary strain rate dependency to be defined.

The Ramberg Osgood relationship [17], describes the deformation of alloys of elasto-plastic property. The non-linear relationship between stress and strain in materials near their yield point is captured in equation 3.

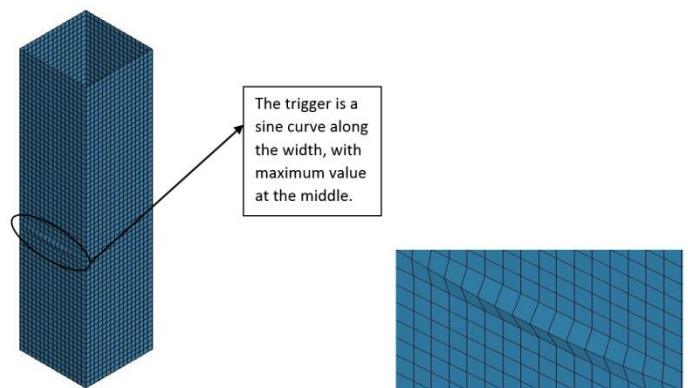


Figure 1: Geometrical Imperfection with trigger mechanism

$$\varepsilon = \frac{\sigma}{E} + K\left(\frac{\sigma}{E}\right)^n \tag{3}$$

where K and n are constants that define the hardening behaviour of the material. σ/E is the elastic part of the strain, and $K(\sigma/E)^n$ is the plastic strain. For ductile materials, the yield offset is often used as the plastic strain at yield. Other forms of this equation can be derived by introducing other parameters.

In Holloman’s equation [18], a power law relationship between stress and plastic strain is also used in describing the plastic behaviour of materials.

$$\sigma = K(\varepsilon_p)^n \tag{4}$$

where K is the strength coefficient, and n is the strain hardening coefficient.

These equations form the basis of the five-parameter model in equation (5). The five-parameter model was used to generate the stress-stain relationship which was implemented using the MAT_ 024 piecewise linear plasticity model.

$$\sigma = \sigma_o + \sum_{i=1}^2 R_i + \sum_{i=1}^2 X_i + \sigma_v \tag{5a}$$

$$R_i = \alpha Q_i [1 - \exp(-C_i \varepsilon_p)] \tag{5b}$$

$$X_i = (1 - \alpha) Q_i [1 - \exp(-C_i \varepsilon_p)] \tag{5c}$$

where σ_o represents the proportionality limit or the yield stress, $\varepsilon_p = \varepsilon - \sigma_o/E$ (ε_p is the effective plastic strain, ε is the total strain and E is the young’s modulus). [19]

The parameter, α , determines the relationship between the kinematic and isotropic hardening. σ_v is the viscous stress and is neglected since aluminium alloys are recognized as almost strain rate insensitive. C_i governs the rate of change of isotropic and kinematic hardening, Q_i is the asymptotic value. These parameters are used because the hardening property is a factor necessary to accurately define the response of the aluminium tubes. For aluminium A6060, the hardening parameter α was found to be 0.7. Hence the material tested shows 70% isotropic hardening and 30% kinematic hardening.[12].

The true stress versus effective plastic strain curve used for this simulation was derived from the material properties presented by [12] as a reasonably accurate property of the aluminium alloy A6060 T4 and T6. Table 1 shows the material properties and figure 2 shows the true stress versus effective plastic strain plot for a 2.5 mm tube.

Table 1: Material Properties for Aluminium A6060 (Langseth *et al.*, 1996)

Parameter	Temper T4			Temper T6		
	1.8 mm	2.0 mm	2.5 mm	1.8mm	2.0mm	2.5mm
σ_o (N/mm ²)	56	66	75	149	152	154
C_1	2326	399.60	25	964.20	861.90	492.40
Q_1 (N/mm ²)	12.56	7.98	75	39.46	35.10	45.39
C_2	15.82	14.54	1.9	14.37	19.29	5.56
Q_2 (N/mm ²)	125.60	135.60	200	57.72	54.00	95.44

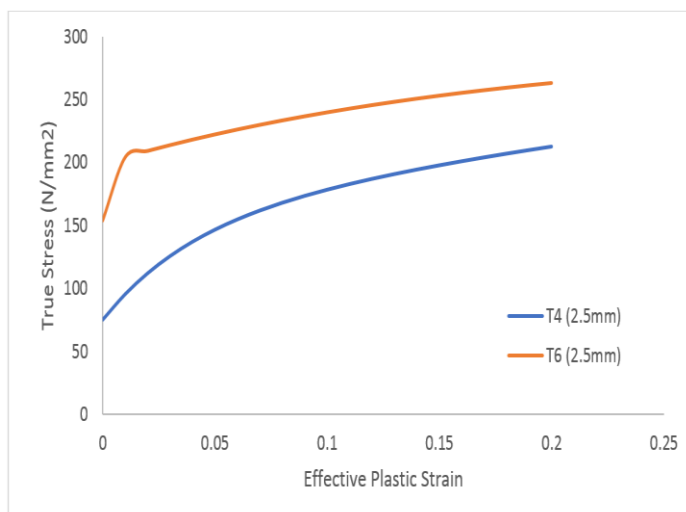


Figure 2: True Stress versus Effective Plastic Strain Curves

The contact between the rigid block and the tube was modelled using the “Automatic node to Surface” option with a coefficient of friction of 0.25. The contact between the lobes during deformation was modelled with a single surface contact algorithm without friction to prevent interpenetration between the folds.

2.4 Quasi-Static Test

The quasi-static loading is a very slow process and was implemented by applying a constant velocity of impact. A load curve was used to apply the load to the tubes at a rate of 10 mm per second in the axial direction of loading (z). The initial length of the tube was 310 mm and the final axial displacement was 250 mm while the simulation time was for 25 s. Initial geometrical imperfection was applied to the tubes as triggers with

amplitude β_0 along the sidewalls, the lower end of the tube was constrained in all directions, and the upper end was given a freedom of motion in the z-direction. To reduce the simulation time, mass scaling was done since LS DYNA is an explicit solver, otherwise the quasi-static loading of the tubes will take enormous time to solve. Hence the mass of the impactor was increased taking note of the effect on the energy absorption and deformation behaviour.

2.4.1 Load curve

The quasi-static loading of the tube was modelled to represent a slow application of the load on the tube. The load was applied at a constant velocity of 10 mm/s as shown in Figure 3.

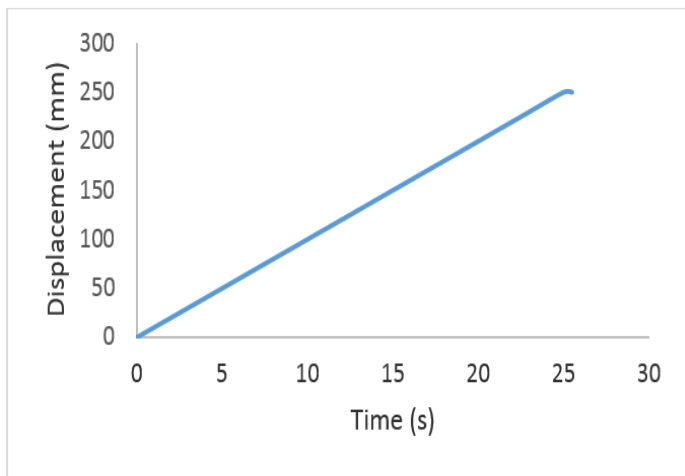


Figure 3: Load curve for quasi-static loading of square tubes

2.4.2 Mass scaling

LS DYNA is primarily based on explicit time integration and running quasi-static simulations takes a long time as the deformation rate is very slow. To perform the quasi-static tests, mass scaling was employed to increase the density of the tubes and impacting mass. The conditions necessary to carry out the mass scaling include:

- Total kinetic energy must be small compared to the total internal energy
- The load-deformation behaviour must be strain rate independent.

The mass density of the tube and the striking mass were increased by different factors from 100 to 10,000 to determine the effect of the mass scaling on the response behaviour of the tube. The crush behaviour of the tubes didn't differ in terms of force-displacement characteristics but the computing time is greatly affected by the mass scaling. Lower scale factors extended the run time of the simulation beyond the bounds of the computing machine.

The mass densities were eventually scaled to 10,000 to arrive at acceptable results within a reasonable computing time.

In validating the accuracy of the model, the quasi-static results will be compared with previous theoretical and experimental works.

2.4.3 Theoretical basis for mean crushing load

Theoretical prediction of the mean crushing load by Abramowicz and Jones [10] for the static loading of square tubes is given as expressed in equation 6.

$$P_m = 13.06\sigma_o t^2 \left(\frac{b}{t}\right)^{1/3} \tag{6}$$

The flow stress values were taken as the average of yield stress and the ultimate stress values for the different tempers and thicknesses.

2.5 Dynamic Test

In the dynamic crushing of the square tubes, the specimen was given the contact definition, boundary condition, material model and element formulation to reflect the conditions as modelled in validated tests. The lower end of the tube was given translational and rotational restraint in all directions to simulate the clamped condition. The impacting mass was constrained in all directions except in the axial direction. This is to prevent unwanted oscillations during contact. The axial loading of the tubes was implemented by applying nodal velocity values for the impacting mass. The termination time was defined according to the duration required for the impacting mass to collapse the tube. The force-displacement history was then plotted to reflect the behaviour of the square tube. Tests were carried out to determine the post buckling behaviour and deformation shapes of the tubes at different impact velocities, impact mass and impact energy.

2.5.1 Dynamic Impact at Constant Velocity

The dynamic effects are examined by carrying out impact tests at 15 m/s for varying mass values from 10 kg to 100 kg. Table 2 presents the load schedule

Table 2: Dynamic Impact load schedule at constant velocity

Mass (kg)	Velocity (m/s)
10	15
25	15
50	15
75	15
100	15

2.5.2 Dynamic Impact at Constant Mass

The effect of varying impact velocity of the mass on the energy absorption, peak force and mean crushing force was also investigated by performing dynamic impact tests on the tube at varying magnitudes of velocity. Table 3 shows the magnitudes of mass and velocity variations used in the tests.

Table 3: Dynamic Impact load schedule at constant mass

Mass (kg)	Velocity (m/s)
50	10
50	15
50	20
50	25

3.0 RESULTS AND DISCUSSION

3.1 Validation of Test Model

The validation of the square tube model used for this investigation is necessary to ensure that the behavior of the specimen reflects established deformation modes and to ensure the result agrees with previous experimental

and theoretical works. Results from the experimental investigation performed by [12] showed that static loading of the tubes resulted in a symmetric lobe formation and the number of lobes was dependent on the temper, as six lobes were observed for temper T4 and seven lobes for temper T6. Figure 4 shows the simulated quasi-static result for the T4 alloy of 2.5 mm thickness characterized by the formed 6 lobes.

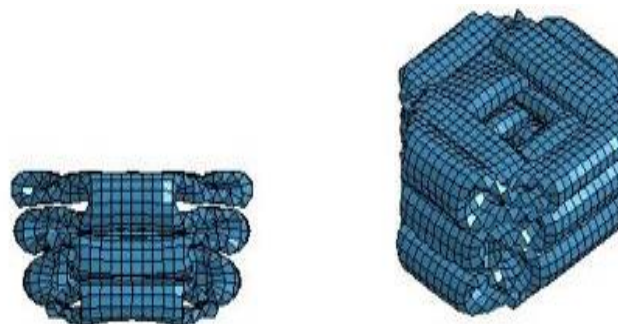


Figure 4: Deformed tube under quasi-static load
Constant Velocity = 10mm/s, Temper = T4, Tube Thickness = 2.5mm

Table 4: Quasi-Static Mean Crushing Force Values

Temper	Thickness (mm)	Theoretical Prediction [Abramowicz and Jones, 1989] (kN)	Experimental Result [Langseth et al., 1996] (kN)	FEA Result(kN)
T4	2.5	32.8	32.4	32.7
	2.0	21.7	20.9	21.9
	1.8	17.2	17.1	17.2
T6	2.5	52.6	45.5	45.2
	2.0	35.6	30.8	31.5
	1.8	29.7	28.1	28.4

Table 4 shows the finite element results for both tempers in this study, compared with theoretical predictions by the Abramowicz and Jones [10] model for predicting the quasi-static mean crushing force, and also the experimental results [12]. The simulation results suggest that the material and geometrical modelling in the numerical set up is well defined.

The geometrical imperfection as a critical factor in determining the deformation mode and energy absorption, is carefully considered to properly represent the quasi-static results in the experimental test. A nodal offset using a single half sine wave with an amplitude of 1 mm along the tube wall, resulted in a force-displacement curve similar to the experimental as shown in Figure 5.

The quasi-static test is a very slow deformation process, so inertia effects are expected to be minimal.

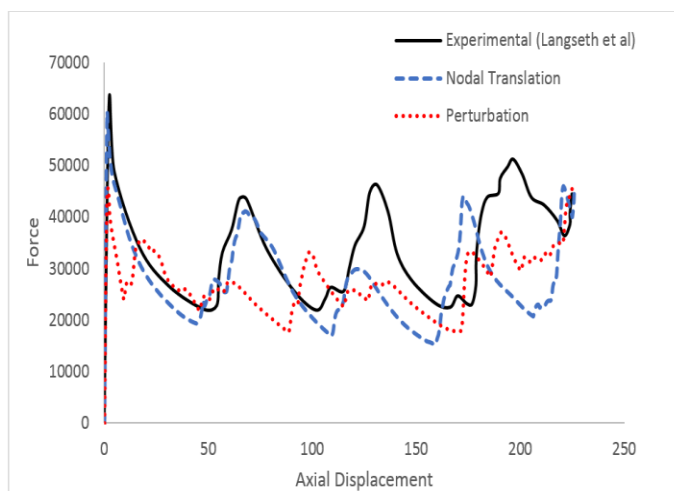


Figure 5: Effect of geometrical imperfection
Constant Velocity = 10mm/s, Temper = T4, Tube Thickness = 2.5mm

In order to optimize the simulation time and initiate the deformation modes similar to experimental tests, trigger mechanisms were implemented. Figures 6 and 7 show the quasi-static test results for T4 and T6. The

plain tube wall without geometrical imperfection is compared with the triggered wall tube specimens with a force-displacement and mean force-displacement plot.

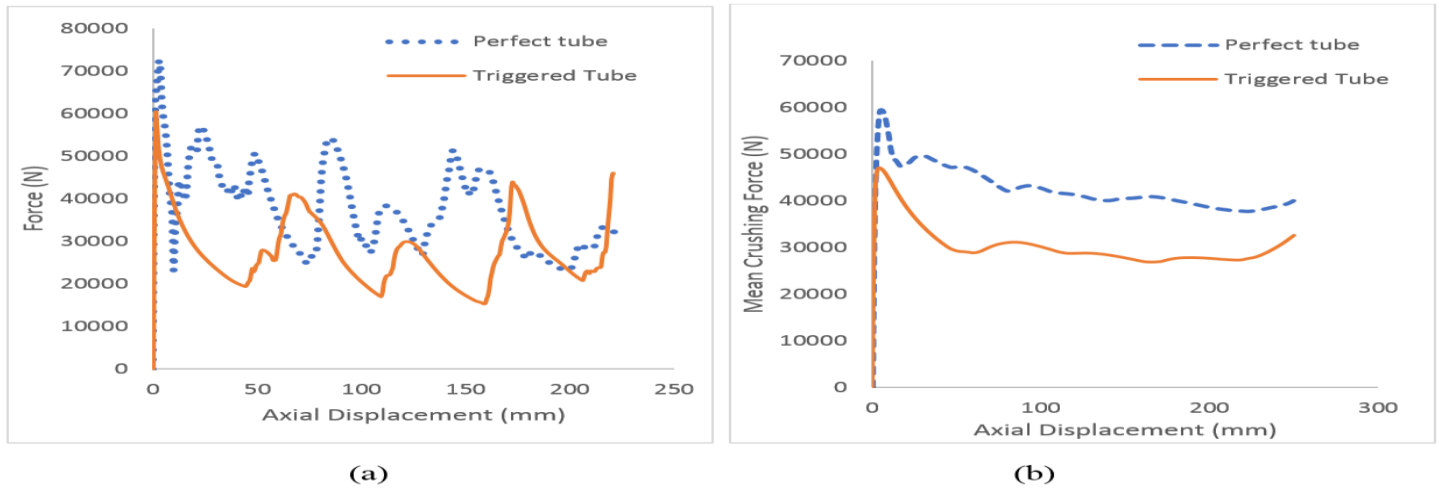


Figure 6: Effect of trigger. (a) Force-displacement. (b) Mean Force-displacement
 Constant Velocity = 10mm/s, Temper = T4, Tube Thickness = 2.5mm

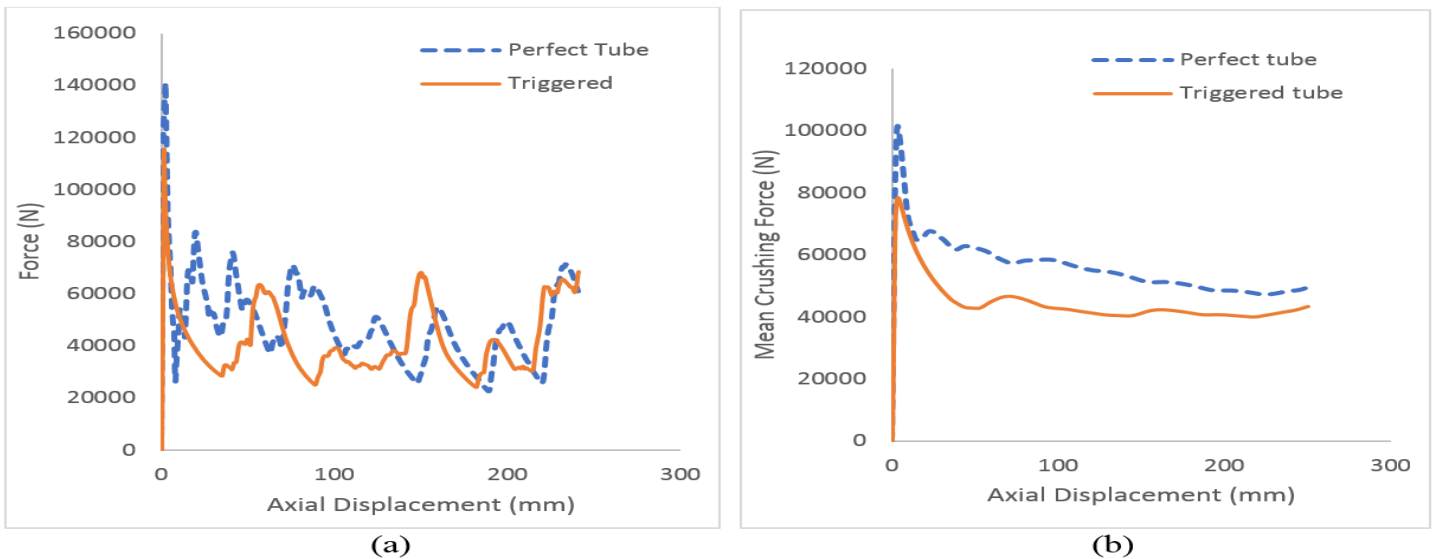


Figure 7: Effect of trigger (T6). (a) Force-displacement. (b) Cumulative Mean Force-displacement
 Constant Velocity = 10mm/s, Temper = T4, Tube Thickness = 2.5mm

The geometrical imperfection, introduced as a trigger along the sidewall of the tube, is responsible for the lowering of the initial peak and cumulative mean force levels in both temper T4 and T6 as shown in figures 6 and 7.

3.2 Dynamic Impact Test

The dynamic behaviour of the tubes under impact load was determined by simulating the axial collapse of the crush tube at constant velocity-varying mass, and then

varying the velocity at constant striking mass. Table 5 presents the numerical results from the dynamic test of the 2.5mm thick tube (T4) at constant impact velocity and varying striking mass.

The simulation result at a constant impact velocity of 15.6 m/s and varying striking mass from 10-100 kg indicates that the peak force level is less affected by the variation in striking mass. However, the energy-absorbed by the tube is expected to increase due to increasing mass magnitude.

Table 5: Dynamic Result for Varying Mass (T4 2.5mm)

Mass (kg)	Velocity (m/s)	Peak Force (kN)
10	15.6	79.8
25	15.6	80.1
50	15.6	81.1
75	15.6	81.1
100	15.6	81.3

The energy increase is evident when the crushing distance of the tube is considered. Figure 8 shows the force-displacement and mean force-displacement plots for the tube specimen (T4), depicting the increase in the crushing distance with increasing striking mass. The rapid increase in the crushing force seen for the 75 Kg and 100 Kg is due to extrusion walls.

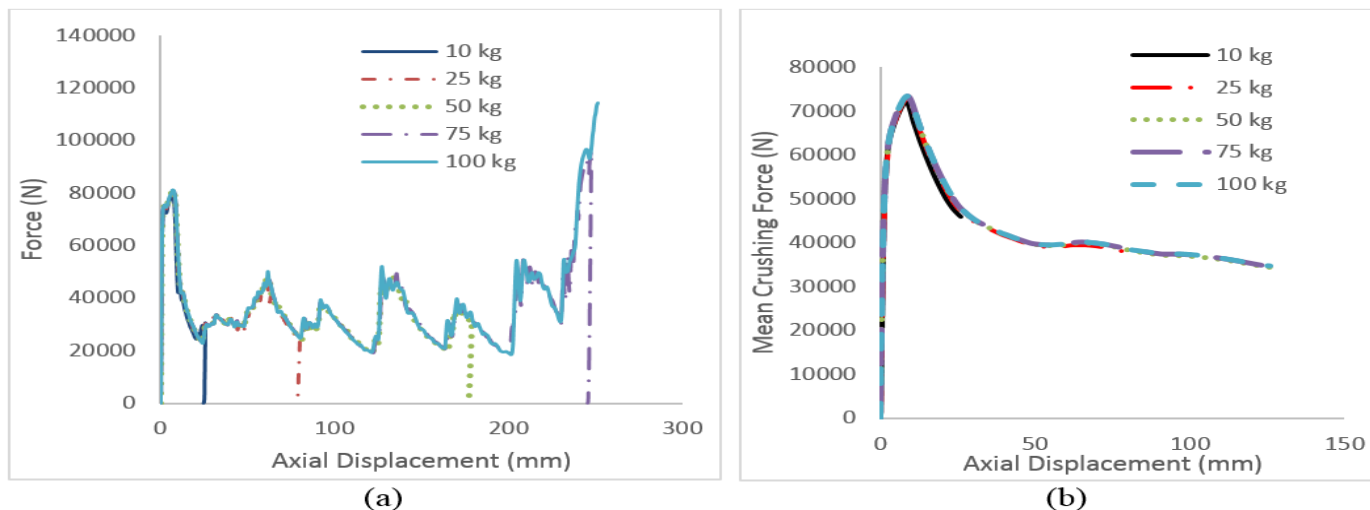


Figure 8. Varying Striking Mass. (a) Force-Displacement (b) Cumulative Mean Force-displacement
Impact Velocity = 15.6m/s, Temper = T4, Tube Thickness = 2.5mm

Furthermore, the dynamic behaviour of the tube was investigated by carrying out dynamic test on tube T4 of 2.5mm thickness at varying velocity values at a constant mass. Table 6 presents the results of the dynamic analysis at a constant impact mass of 50 kg and velocity from 10 to 25 m/s.

Table 6: Dynamic Results for Varying Impact Velocity (T4 2.5mm)

Mass (kg)	Velocity (m/s)	Peak Force (kN)
50	10	76.5
50	15	80.8
50	20	84.8
50	25	89.9

The dynamic result from table 6 shows that the peak force increases as the velocity of impact increases. Also, the force-displacement plots on figure 9 show that the crushing distance also increases with increasing impact velocity. Densification was observed at displacements above 250mm for tubes tested at 20m/s and 25m/s resulting in elevated force towards the end if the simulation, these exaggerated force values were not included in the plot data.

The simulation result at a constant impact velocity of 15.6 m/s and varying striking mass from 10-100 kg indicates that the peak force level is less affected by the variation in striking mass. However, the energy-absorbed by the tube is expected to increase due to increasing mass magnitude.

The increase in the peak and mean force levels in the dynamic test implies an increase in strength of the tube. This improved strength is illustrated in the Von Mises stress distribution plot for the two tests at same crushing distance of 50mm.

The formation of the first lobe completes at 50mm. The stress level across the tube sidewall is higher for the dynamic loading compared to the quasi-static loading at the same crush distance as shown in figure 11. This is due to the resistance (inertia) initiated in the dynamic case as a result of the deceleration of the impacting mass.

For the T6 alloy, the quasi-static progressive buckling continues till the bottoming out of the tube as shown in figure 12, while the dynamic condition predicts a rebound of the impacting mass at t = 0.016 seconds as shown in figure 13. The Stress range is also compared for at a crush distance of 50 mm in figure 14.

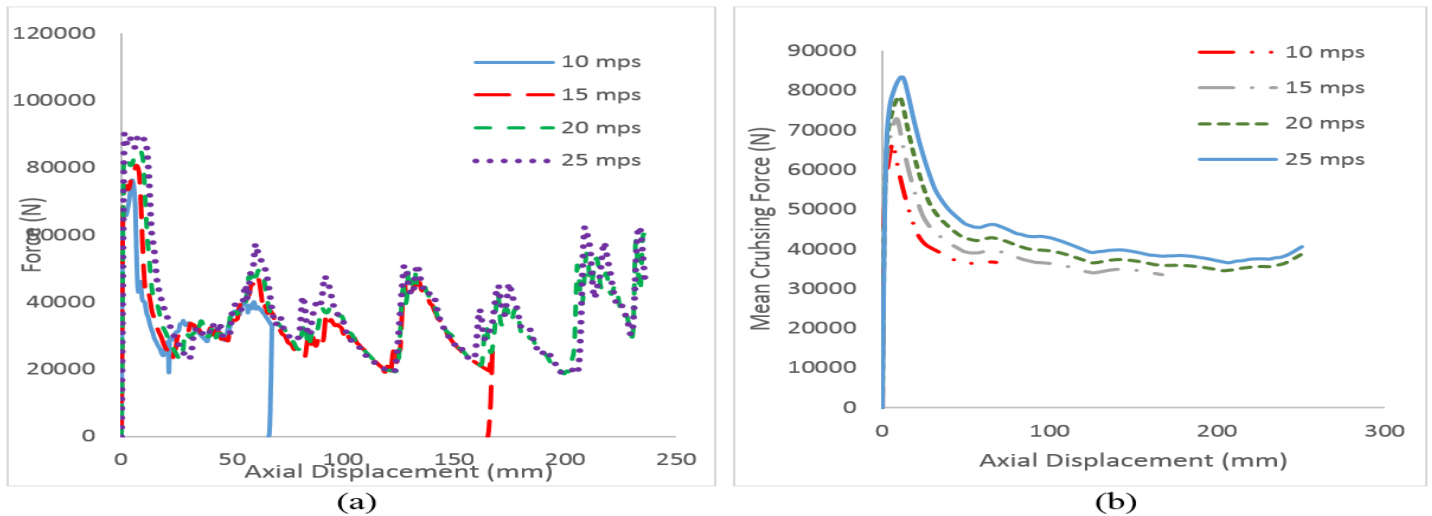


Figure 9: Varying Impact Velocity (a) Force-Displacement (b) Mean Force-displacement
 Impact mass = 50kg, Temper = T4, Tube Thickness = 2.5mm

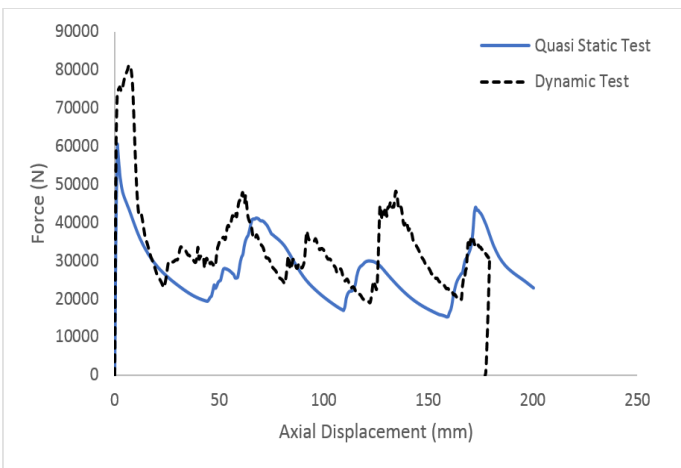


Figure 10: Dynamic and Static Test
 Impact mass = 52.92 kg, Impact Velocity = 15.6m/s, Temper = T4, Tube Thickness = 2.5mm

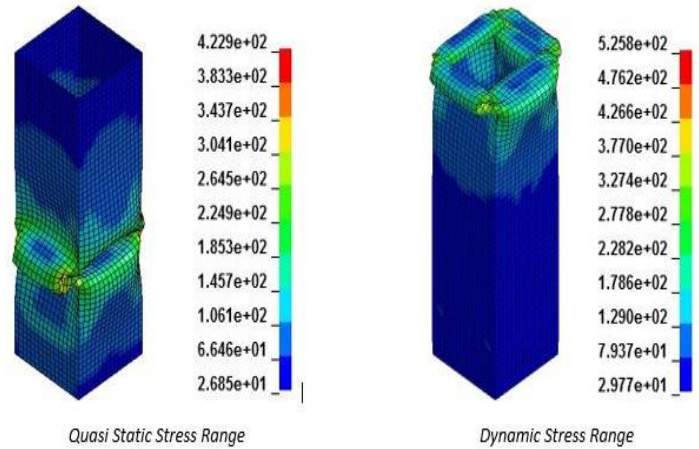


Figure 11: Stress Distribution at 50mm Crush Length
 Impact mass = 52.92 kg, Impact Velocity = 15.6m/s, Temper = T4, Tube Thickness = 2.5mm

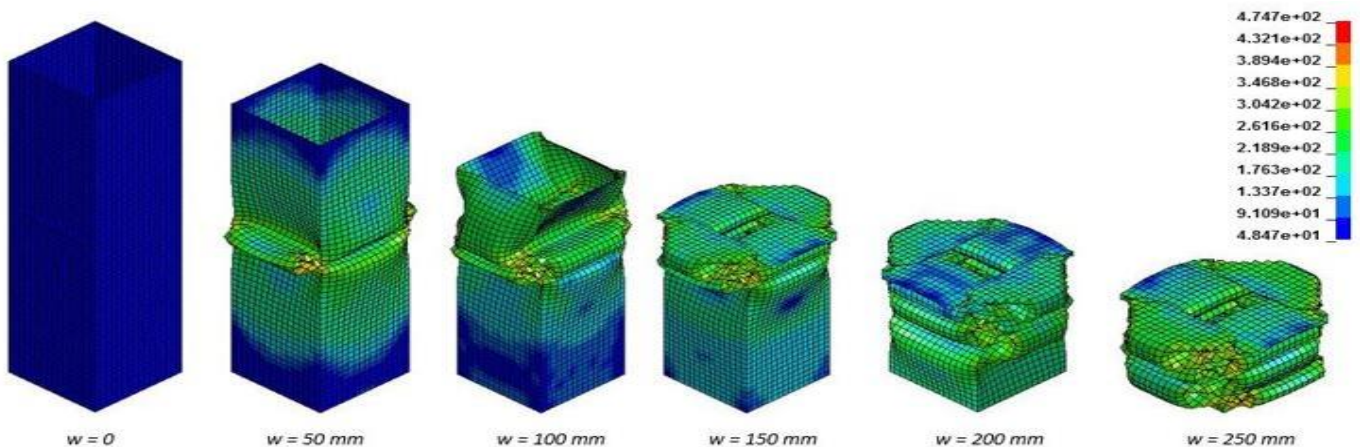


Figure 12: Quasi Static Stress Distribution
 Impact mass = 50kg, Temper = T6, Tube Thickness = 2.5mm

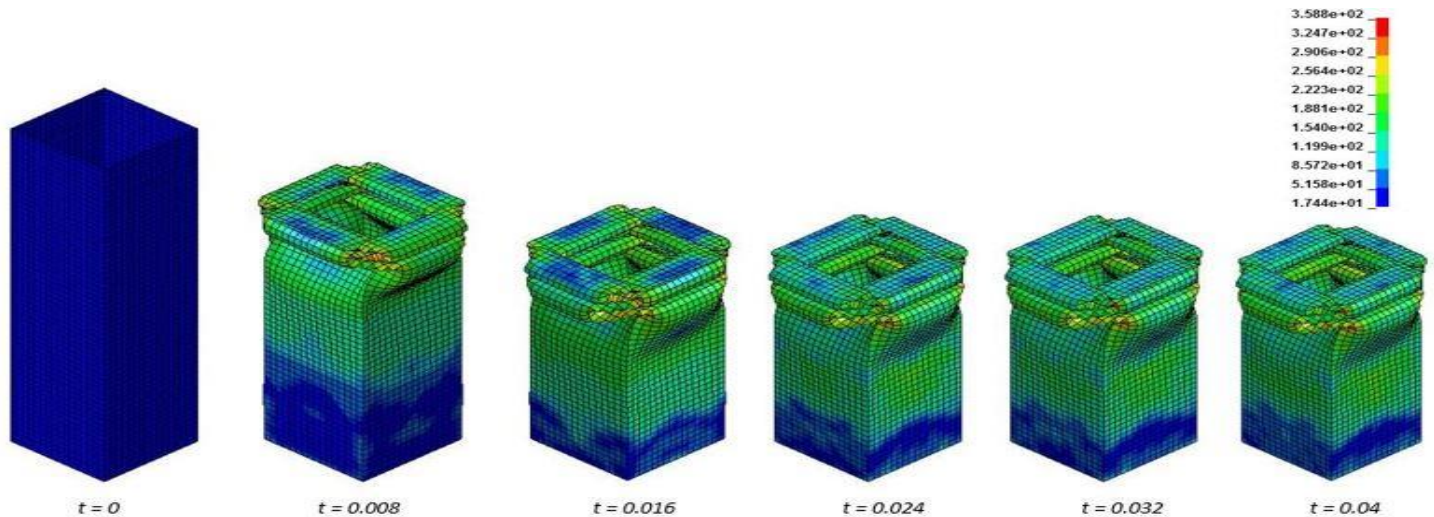


Figure 13: Dynamic Stress distribution
Impact mass = 52.92 kg, Impact Velocity = 15.6m/s, Temper = T6, Tube Thickness = 2.5mm

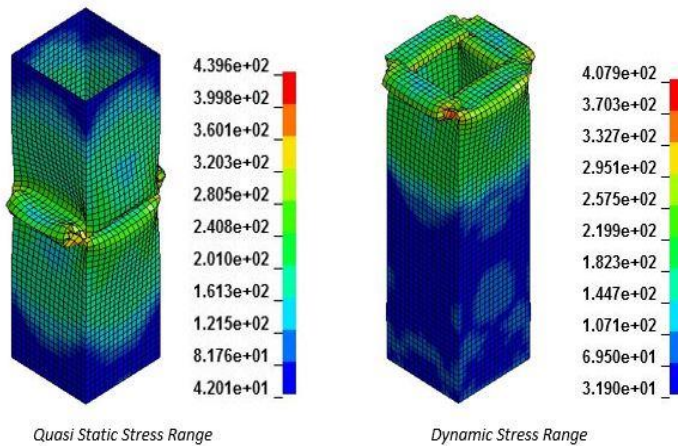


Figure 14: Stress Distribution at 50mm Crush Length
Impact mass = 52.92 kg, Impact Velocity = 15.6m/s, Temper = T6, Tube Thickness = 2.5mm

Figure 14 shows that the dynamic stress range is lower than the stress range for quasi-static loading. This result shows that the stress distribution may portray dynamic force increase or reduction depending on thickness and temper of the tube being examined because both tempers exhibit a different pattern when both loading conditions are compared. This suggests the force-displacement behaviour is a superior metric for comparing energy absorption in tubes

3.3 Shell Thickening and Lateral Inertia

The magnitude of the thickness of the tube wall is examined through the simulation time to unravel how the variation in wall thickness affects lateral inertia and consequently, the deformation behaviour of the tube in a dynamic crush. The variation in tube wall thickness is compared for the dynamic and quasi-static crushing. Also, the tube thickness variation under increasing impact velocity in the dynamic case.

Figure 15 shows that during the quasi-static loading, the tube thickness remains relatively constant at the initial tube thickness of 2.5mm while the dynamic loading induces a thickening of the tube wall at the beginning of the deformation before the progressive buckling commences. The thickness of the tube rapidly increases at the beginning of the deformation, resisting the motion of the impacting mass. The tube thickness increases from 2.5 mm to 2.59 mm, which is about a 3.42% increase for a dynamic loading at 15m/s. The effect of lateral inertia on the tube is further explored by comparing the tube thickness magnitudes at increasing impact velocities.

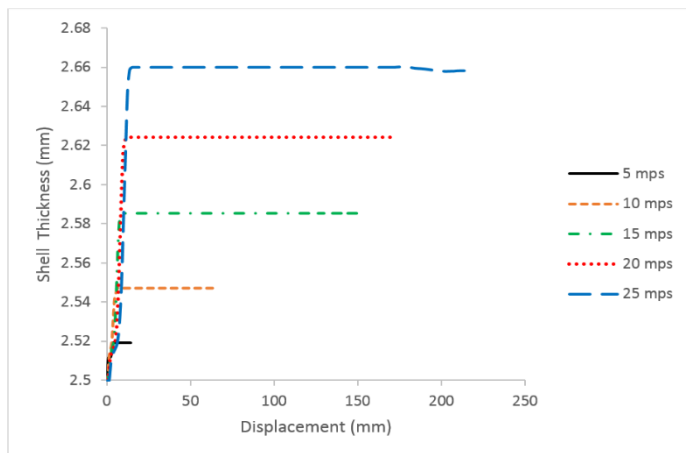


Figure 15: Inertia Effects on Tube Thickness at 15m/s
Impact mass = 52.92 kg, Impact Velocity = 15m/s, Temper = T4, Tube Thickness = 2.5mm

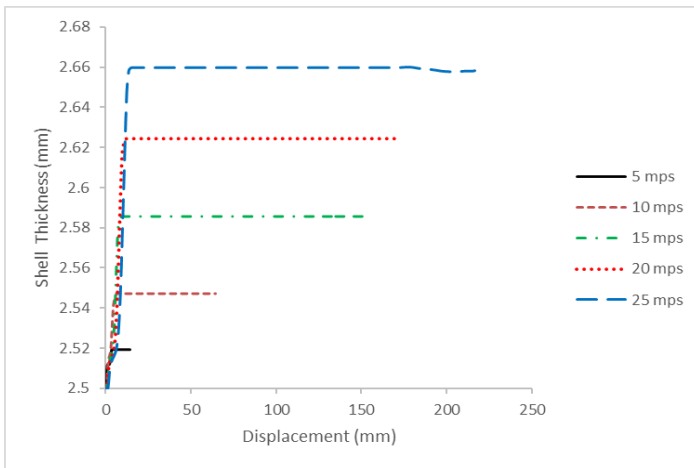


Figure 16: Inertia Effects on Tube Thickness
Impact mass = 50kg, Temper = T4, Initial Tube Thickness = 2.5mm

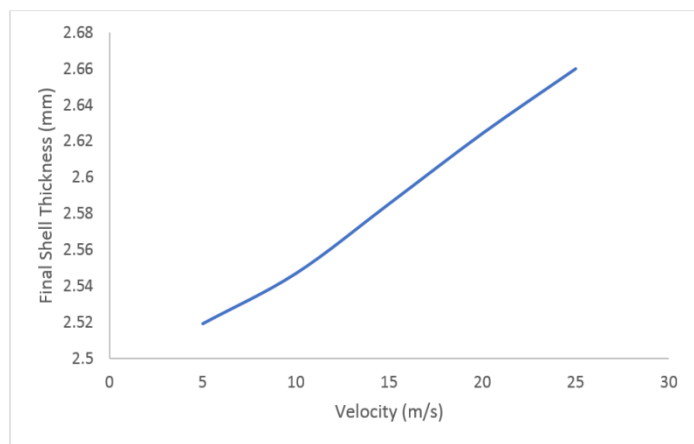


Figure 17: Final Thickness Versus Velocity (Dynamic Loading)
Impact mass = 50kg, Temper = T4, Initial Tube Thickness = 2.5mm

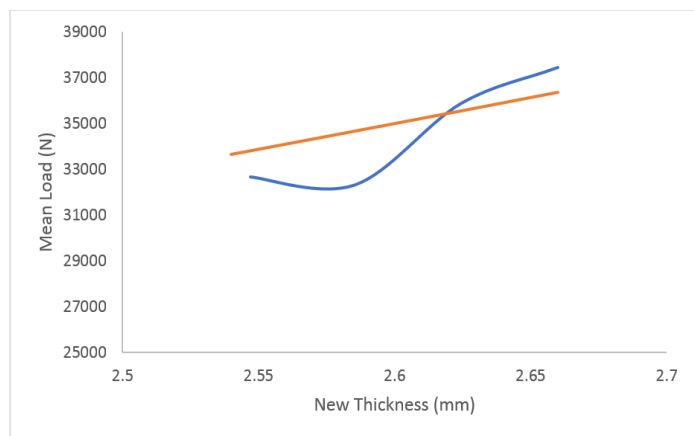


Figure 18: Mean Crushing Force-Thickness
Impact mass = 50kg, Temper = T4, Initial Tube Thickness = 2.5mm

Figures 16 and 17 present the shell thickness-displacement and final shell thickness-velocity plot for the

tubes at velocities from 5-25 m/s respectively. The results show that the shell thickness is an increasing function with increasing impact velocity. Higher impact velocities will result in higher tube thickness and essentially, more energy absorption by the tube. The thickening of the tube wall at the instant of impact is responsible for the inertia resisting the motion of the impacting mass. As depicted in figure 16, the thickness of the tube increases at the very beginning of the deformation even though the shell thickness was measured at the bottom-most element of the shell

Figure 18 shows the mean crushing force versus new thickness plot for the dynamic loading condition, having established that an increase in impact velocity will result in an increase in the cumulative mean crush force of the tube; the cumulative mean force is then plotted against the new shell thickness values at the various impact velocities (10 to 25m/s). The mean force calculated at different thickness values (2.5mm to 2.67mm) using equation (6) is also plotted in figure 18. At lower velocities, the tubes are subjected to lower impact energy levels, therefore the cumulative mean force data set only captures force levels closer to the initial peak force, resulting in higher cumulative mean force values. The cumulative mean force at the plateau region of the force-displacement curve becomes significant after 15m/s (Figure 9). This explains the initial dip on the plot. However, the result shows a general trend of the cumulative mean force increasing with an increase in the wall thickness value. This implies that the lateral inertia which is responsible for the crush force increase of the tube specimen in the dynamic test, is a consequence of the tube thickening that occurs at the instance of impact. A further explanation for thickening is that, at higher impact velocities, there is more compressive axial deformation of the tube walls during impact than at lower impact velocities.

Furthermore, the theoretical model of Abramowicz and Jones [20] also shows in figure 18, linearly increasing relationship between the mean crushing force and various wall thickness values of the tubes. The range of increase in forces levels are also seen to be close to the numerical results. This indicates that shell thickening is a phenomenon in the dynamic crushing of energy absorbing members, particularly aluminium square tubes, that is related to lateral inertia leading to dynamic cumulative mean force increase.

4.0 CONCLUSION

From the numerical results of the axial crushing of the specimens, the following conclusions can be deduced:

- i. Dynamic tests results show an increasing function between impact mass and energy absorption at constant impact velocity. Although, the effect is only significant on the crushing distance, the peak force values are barely affected by the increase in mass. Increasing the impact velocity (at constant mass) results in an increased energy absorption which significantly affects the crushing distance, peak and mean force values. This implies that the impact velocity influences the energy absorption characteristics of the crush tube more than the impact mass.
- ii. The dynamic loading condition results in an increased peak and mean crushing force level compared with the quasi-static case. The dynamic loading results in a deformed structure with up to 34.3% increased peak force.
- iii. Lateral inertia is a consequence of the shell thickening initiated at the onset of the deformation of the square tube walls. A 3.4% increase in thickness was observed for the 2.5 mm thick tube subjected to a 15m/s impact speed. This is found to increase as the impact velocity increases. In the design of energy absorbing structures to enhance the crashworthiness of automotive structures, shell thickening of the crush tubes and the resulting lateral inertia must be taken into consideration to ensure optimum performance.
- iv. Geometrical Imperfection is a significant factor in the formation of the deformation modes and crush characteristics of the tubes. It is therefore essential to carefully define the stochastic fields or nodal offsets to accurately simulate the crush behaviour achieved in experimental tests. Deliberate inclusion of weak points in the crush tube to induce gradual crushing of the tube will be considered in future works to reduce peak crushing force in order to reduce peak deceleration.
- v. Future work can consider the axial strains in elements during impact.

REFERENCES

- [1] N. Hashimoto, "Application of Aluminum Extrusions to Automotive Parts," *Kobelco Technology Review*, 35, 2017.
- [2] T. Thongtip and S. Chanthanumataporn, "Crashworthiness Investigation of Multi-stage Structures Designed for Underrun Protection Devices," *Applied Science and Engineering Progress*, 2020.
- [3] L. Hou et al., "An integrated multi-objective optimization method with application to train crashworthiness design," *Structural Multidisciplinary Optimization*, 2020.
- [4] H. Mou, J. Xie, Y. Liu, K. Cheng, and Z. Feng, "Impact test and numerical simulation of typical sub-cargo fuselage section of civil aircraft," *Aerospace Science and Technology*, 1, p. 106305, 2020.
- [5] P. Hernalsteen and L. C. Leblois, "The use of energy absorbers to protect structures against impact loading," *Nuclear Engineering and Design*, 37(3), 1976, pp. 373–406.
- [6] M. Samuelides, "Recent advances and future trends in structural crashworthiness of ship structures subjected to impact loads," *International Journal of Impact Engineering*, 5302(20), 2015,
- [7] J. M. Alexander, "An approximate analysis of the collapse of thin cylindrical shells under axial loading," *Journal of Mechanics and Applied Mathematics*, 13(1), 1960, pp. 10–15.
- [8] W. Abramowicz, "The effective crushing distance in axially compressed thin-walled metal columns," *International Journal of Impact Engineering*, 1(3), 1983, pp. 309–317.
- [9] T. Wierzbicki and W. Abramowicz, "On the Crushing of thin Walled Structures," *Journal of Impact Engineering*, 5(10), 1983, pp. 2–4, 1983.
- [10] W. Abramowicz and N. Jones, "Dynamic axial crushing of circular tubes," *International Journal of Impact Engineering*, vol. 2, no. 3, 1984, pp. 263–281.
- [11] M. Langseth, O. S. Hopperstad, and A. G. Hanssen, "Crash behaviour of thin-walled aluminium members," *Thin-Walled Structures*, 32(1–3), 1998, pp. 127–150, 1998.
- [12] M. Langseth and O. S. Hopperstad, "Static and dynamic axial crushing of square thin-walled aluminium extrusions," *International Journal of Impact Engineering*, 18(7), 1996, pp. 949–968.
- [13] D. Karagiozova and N. Jones, "Inertia effects in square tubes subjected to an axial impact," pp. 1–10, 2002.
- [14] Q. Fang, J. Zhang, Y. Zhang, H. Wu, and Z. Gong, "A 3D mesoscopic model for the closed-cell metallic foams subjected to static and dynamic loadings,"

- International Journal of Impact Engineering*, pp. 1–10, 2014.
- [15] K. Praveen and S. Shrivathsav, “Influence of forming parameters on the crash performance of capped cylindrical tubes using LS - DYNA follow - on simulations,” *International Journal on Interactive Design and Manufacturing*, 123456789, 2019.
- [16] M. Khadyko, S. Dumoulin, T. Børvik, and O. S. Hopperstad, “Simulation of large-strain behaviour of aluminium alloy under tensile loading using anisotropic plasticity models,” *Computers & Structures*, 157, pp. 60–75, 2015.
- [17] M. Gajjar and H. Pathak, “Elasto-Plastic Fracture Modeling for Crack Interaction with XFEM,” *Transaction of Indian Instrument and Metals*, 2020.
- [18] R. K. Nutor, N. K. Adomako, and Y. Z. Fang, “Using the Hollomon Model to Predict Strain-Hardening in Metals,” 2(1), pp. 1–4, 2017.
- [19] M. Langseth, O. S. Hopperstad, and T. Berstad, “Crashworthiness of aluminium extrusions: validation of numerical simulation, *elect of mass ratio and impact velocity*,” 22(734), 1999.
- [20] W. Abramowicz and N. Jones, “Dynamic Progressive Buckling of Circular and Square Tubes,” *International Journal of Impact Engineering*, 4(4), pp. 243–270, 1986.